RESEARCH ARTICLE

AAV.Dysferlin Overlap Vectors Restore Function in Dysferlinopathy Animal Models

Patricia C. Sondergaard[1], Danielle A. Griffin[1], Eric R. Pozsgai[1,2], Ryan W. Johnson[1], William E. Grose[1], Kristin N. Heller[1], Kim M. Shontz[1], Chrystal L. Montgomery[1], Joseph Liu[1], Kelly Reed Clark[1,2], Zarife Sahenk[1,3,4], Jerry R. Mendell[1,3,4] & Louise R. Rodino-Klapac[1,2,3]

[1]Center for Gene Therapy, Nationwide Children's Hospital, Columbus, Ohio
[2]Biomedical Sciences Graduate Program, The Ohio State University, Columbus, Ohio
[3]Department of Pediatrics, The Ohio State University, Columbus, Ohio
[4]Department of Neurology, The Ohio State University, Columbus, Ohio

Correspondence

Louise R. Rodino-Klapac, The Research Institute at Nationwide Children's Hospital, 700 Children's Dr., Room WA3021, Columbus, OH 43205. Tel: 614-722-2678; Fax: 614-722-3273; E-mail: Louise.Rodino-Klapac@nationwidechildrens.org

Data and materials availability: AAVrh.74.DYSF.DVs is the property of Nationwide Children's Hospital and must be obtained through an MTA.

Abstract

Objective: Dysferlinopathies are a family of untreatable muscle disorders caused by mutations in the dysferlin gene. Lack of dysferlin protein results in progressive dystrophy with chronic muscle fiber loss, inflammation, fat replacement, and fibrosis; leading to deteriorating muscle weakness. The objective of this work is to demonstrate efficient and safe restoration of dysferlin expression following gene therapy treatment. **Methods**: Traditional gene therapy is restricted by the packaging capacity limit of adeno-associated virus (AAV), however, use of a dual vector strategy allows for delivery of over-sized genes, including dysferlin. The two vector system (AAV.DYSF.DV) packages the dysferlin cDNA utilizing AAV serotype rh.74 through the use of two discrete vectors defined by a 1 kb region of homology. Delivery of AAV.DYSF.DV via intramuscular and vascular delivery routes in dysferlin deficient mice and non-human primates was compared for efficiency and safety. **Results**: Treated muscles were tested for dysferlin expression, overall muscle histology, and ability to repair following injury. High levels of dysferlin overexpression was shown for all muscle groups treated as well as restoration of functional outcome measures (membrane repair ability and diaphragm specific force) to wild-type levels. In primates, strong dysferlin expression was demonstrated with no safety concerns. **Interpretation**: Treated muscles showed high levels of dysferlin expression with functional restoration with no evidence of toxicity or immune response providing proof of principle for translation to dysferlinopathy patients.

Introduction

Dysferlinopathies are a family of disorders caused by autosomal recessive mutations in the dysferlin (DYSF) gene. These disorders include limb girdle muscular dystrophy type 2B (LGMD2B),[1] Miyoshi Myopathy (MM1),[2] and distal anterior compartment myopathy,[3–5] among others.[1–3,6] LGMDs comprise 30% of all progressive muscular dystrophies with LGMD2B as the most frequently diagnosed dysferlinopathy.[7,8] Mutations in DYSF lead to a progressive muscular dystrophy with chronic muscle fiber loss, inflammation, fat replacement, and fibrosis, all contributing to deteriorating weakness.[7] In general, patients present with an abrupt onset in the second decade with progressive involvement of proximal and distal musculature.[9,10] Although dysferlinopathies are slowly progressing disorders, approximately one-third of patients become wheelchair-dependent within 15 years of disease onset.[7,10] There is no cure for these diseases and limited treatment options are available. Even use of steroids, which have

been previously successful for Duchenne muscular dystrophy patients, is ineffective and not warranted.[11] Although it has been occasionally reported that treatment with IV-IG or rituximab therapies can be effective by modifying the immune response, to date there remains no cure.[12,13] Thus, the need for a treatment is clear.

The DYSF gene consists of 55 exons encompassing 150 kb of genomic DNA.[14] The associated cDNA is ~6.5 kb and codes for the dysferlin protein.[2,14–16] Dysferlin, a member of the ferlin family, is composed of seven N-terminal C2 domains with a transmembrane C-terminus.[17,18] Dysferlin has multiple roles in skeletal muscle including sarcolemmal membrane repair,[16,19,20] vesicle trafficking,[21] t-tubule structure and function[22] and endocytosis.[23] Our group[16] and others[19,20,24] have studied the role of dysferlin in Ca^{2+}-dependent membrane repair, consistently reporting a decrease in dysferlin-deficient fiber sarcolemmal resealing following acute injury. As skeletal muscle is mechanically active, this deficit in repair leads to regeneration/degeneration of fibers with muscle fiber necrosis/loss, and progressive limb weakness.[19,20]

Recent years have shown profound development of adeno-associated viral (AAV) gene transfer.[16,25–28] Although there was some reported plasticity,[29,30] the packaging limit of AAV is 4.7 kb, requiring the development of cDNA cassettes within this constraint. Groups have reported the use of miniaturized genes and trans-splicing approaches; however, reduced gene expression and protein function hinder the technology.[31–34] In our previous work, we delivered full-length DYSF using AAV5 delivery of partially packaged 5′ and 3′ fragments of the dysferlin containing expression cassette.[16] Southern blot revealed that all encapsidated DNA was ≤~5.2 kb in length.[16] Overlapping homologous sequences facilitated reconstitution of full-length DYSF. As the packaging in AAV5 was uncontrolled, it became desirable to develop a strategy for packaging of discrete, well-identified constructs. From our experience and that of others,[16,35,36] we used a dual vector strategy using co-injection of two vectors.

To accomplish efficient gene expression, we split the dysferlin cDNA into two segments with a 1 kb overlap region and packaged them into separate cassettes within AAVrh.74. Upon co-injection, the two cDNA segments provide a substrate for homologous recombination or repair [29,37,38] to recover the full-length gene. In our studies, the dual vector strategy demonstrates higher levels of gene expression than previous work with AAV5.DYSF.[16] In addition, membrane repair capacity and diaphragm specific force in the dysferlin knock-out mouse model were restored to wild-type (WT) levels. Following demonstration of robust dysferlin expression in mice we performed injections in rhesus macaques (nonhuman primates [NHPs]) to validate a safety profile for the dual vector treatment.[39] We found no toxicity following AAVrh74.DYSF.DV in NHPs. Taken together with functional outcome measures in dysferlin deficient mice, AAVrh.74.DYSF.DV is well-positioned for translation to dysferlinopathy patients.

Materials and Methods

Dysferlin gene construction

For all gene transfer studies, human dysferlin cDNA (Genbank# NM_003494.3) was used. The full-length dysferlin cassette was made as previously described.[16] The dual vector dysferlin cassettes were generated to encompass the 5′ or the 3′ portion of the full-length dysferlin cassette.[16] The 5′ cassette contains the MHCK7 promoter, the chimeric intron and the first 3370 bp of the dysferlin cDNA flanked by AAV2 ITRs. The 5′ plasmid, pAAV.MHCK7.DYSF5′.PTG, was generated through a NotI restriction enzyme digest on the original pAAV.MHCK7.DYSF plasmid, removing the entire dysferlin cDNA. The 5′ portion of the dysferlin cDNA was then polymerase chain reaction (PCR) amplified using the primers 5′ F – TGCGGAATTGTACCCGCGGCCGCGGC-TAGCCACCAT and 5′ R – TAAAGATCTTTTATTGCGG-CCGCCCTCAAGGGCAAACACAGCTG and then cloned into the NotI digested vector using the ClonEZ PCR Cloning kit (Genscript Piscataway, NJ USA), forming the plasmid pAAV.5′DYSF. Both constructs were fully sequenced to confirm plasmid fidelity. For gene transfer studies in NHPs, the 5′ vector genome (vg) includes a FLAG tag after the Kozak sequence and before the start of the dysferlin 5′ cDNA. The FLAG tag is used for differentiation of endogenous and delivered dysferlin.

The 3′ vector, pAAV.DYSF3′.POLYA, was generated by performing a PmeI/Tth111I double restriction enzyme digest on pAAV.MHCK7.DYSF which removed the entire promoter, chimeric intron, and 2407 bp of the 5′ portion of the dysferlin cDNA from the vector. The remaining vector was end-repaired and ligated to form the plasmid containing the remaining 3866 bp of the dysferlin cDNA also including the native 3′UTR/polyA sequence. Sequencing was performed to confirm the removal of the 5′ portion of the dysferlin cassette.

AAV vector production

pAAV.MHCK7.DYSF was packaged into AAV serotype 5 as previously described.[16] pAAV.MHCK7.DYSF5′.PTG and pAAV.DYSF3′.PolyA were packaged into AAV serotype Rh74 capsid using the standard triple transfection protocol.[16] A quantitative PCR-based titration method

was used to determine an encapsulated vg titer utilizing a Prism 7500 Fast Taqman detector system (PE Applied Biosystems Grand Island, NY USA).[40] The following primers/probes were used: AAVrh.74.MHCK7.DYSF5′. PTG – F primer – CCAACACCTGCTGCCTCTAAA, R primer – GTCCCCCACAGCCTTGTTC, Probe – TGGA TCCCCTGCATGCGAAGATC; AAVrh.74.DYSF3′.PolyA – F primer – AGATCACCCCACTTCCATCATT, R primer – TGAAATATGTCTGAGCTGATCCAAA, Probe – CCTT CTCCCCCAACCCAACGCT.

Animal models

Dysferlin deficient mouse strains

Stocks of C57BL/10, 129-Dysf$^{-/-}$, and Bla/J mice were bred and maintained as homozygous animals in standardized conditions in the Animal Resources Core at the Research Institute at Nationwide Children's Hospital. Bla/J mice were generously provided by the Jain Foundation. Mice were maintained on Teklad Global Rodent Diet (3.8z5 fiber, 18.8% protein, 5% fat chow) with a 12:12 h dark:light cycle. Procedures used in experiments were approved by the Institutional Animal Care and Use Committee at Nationwide Children's Hospital (protocol AR08-00017).

Nonhuman primates

Vendors provided serum from rhesus macaques before animal purchase for determination of AAVrh.74 binding antibody titers. Sero-negative animals (categorized by <1:50 total antibody titer dilution via enzyme-linked immunosorbent assay [ELISA]) were obtained and housed in twos or threes to promote socialization in the Animal Resources Core at the Research Institute at Nationwide Children's Hospital. All procedures were approved by the Institutional Animal Care and Use Committee at Nationwide Children's Hospital (protocol AR06-00116).

In vivo gene delivery

Intramuscular delivery

The anterior compartment, containing the tibialis anterior (TA) and extensor digitorum longus (EDL) muscles, of the lower left limb of 4–6 week old 129-Dysf KO (Dysf$^{-/-}$) mice were injected with 1×10^{11}vg of AAVrh.74.-MHCK7.DYSF5′.PTG and 1×10^{11}vg of AAVrh.74.-DYSF3′.PolyA diluted in normal saline buffer (2×10^{11}vg total dose in 50 μL volume) ($n = 4$ per timepoint). Control mice were injected with only AAVrh.74.MHCK7.-DYSF5′.PTG, AAVrh.74.DYSF3′.PolyA or normal saline.

TA muscles from both limbs were removed at 1, 3, or 6 months postinjection to assess gene transfer efficiency. All organs and various muscles were harvested for analysis of biodistribution of vgs.

The flexor digitorum brevis (FDB) muscle of 8 week old 129-Dysf$^{-/-}$ mice were injected with 6×10^{9}vg, 2×10^{10}vg, or 6×10^{10}vg total dose of AAVrh.74.DYSF in normal saline buffer (1:1 ratio of AAVrh.74.MHCK7.-DYSF5′.PTG and AAVrh.74.DYSF3′.PolyA, total volume of 30 μL). Six mice per dose were treated. The FDB was removed 12 weeks postinjection and used for membrane repair assay (see below).

For long-term expression studies, 4 week old Dysf$^{-/-}$ mice were injected in the left TA with 2×10^{11}vg AAV5.MHCK7.DYSF and sacrificed at 1, 3, 6, 9, or 12 months ($n = 4$ per timepoint).

For studies in NHPs ($n = 3$), the left TA was injected with 5×10^{12}vg total dose of AAVrh.74.DYSF.DV. Right TA was used as a contralateral control and was injected with normal saline.

Regional vascular delivery

129-Dysf KO mice at 4–6 weeks of age were perfused with 1×10^{12}vg AAVrh.74.MHCK7.DYSF5′.PTG and 1×10^{12}vg AAVrh.74.DYSF3′.PolyA (total dose 2×10^{12}vg in 100 μL normal saline) as previously described.[41] Briefly, mice were anesthetized and the femoral bundle was visualized via a small incision proximal to the mid-thigh. Arterial blood flow was controlled by catheter placement using a customized heat pulled polypropylene 10 (PE-10) catheter. Prior to vector administration, the arterial catheter was flushed (preflush) with 100 μL sterile normal saline. Immediately prior to vector administration all blood flow to the extremity was impeded (isolated limb perfusion – ILP) by tightening the ligature at the mid-thigh. AAVrh.74.DYSF.DV was perfused through the femoral artery in 100 μL administered at a rate of ~2 μL per second (over 60–80 sec). After 10 min of maintained vascular occlusion, 100 μL of normal saline was administered to the arterial catheter (again at about 2 μL per second) as a postflush and the tourniquet was then released. The wound was flushed with sterile normal saline and closed with a 6-0 proline suture. Four weeks postinjection, animals ($n = 4$) were sacrificed and muscles (TA, gastrocnemius, EDL) were extracted for analysis of dysferlin expression.

Systemic delivery

Systemic delivery of AAVrh.74.DYSF.DV was achieved through tail vein injection of 2×10^{12}vg or 6×10^{12}vg (1:1 ratio of AAVrh.74.MHCK7.DYSF5′.PTG and

AAVrh.74.DYSF3′.PolyA, total volume of 150 μL) into 8 week old Bla/J mice ($n = 6$ per dose). Mice were sacrificed 12 weeks postinjection with a full necropsy performed. The diaphragm was subjected to force measurements (see below), the FDB was tested for membrane repair ability and muscles and organs were harvested for expression and histopathology.

For histological analysis all muscles and organs (unless used for membrane repair) were embedded in 7% gum tragacanth and flash frozen in liquid nitrogen cooled isopentane. Frozen sections (12 μm) were collected for immunohistochemistry and western blot analysis.

Membrane repair assay

The ability of muscle membrane to repair following injury was assessed on muscle fibers isolated from FDB muscles using treatment with a 2% collagenase Type I solution. Fibers were washed in PBS (phosphate-buffered saline) and placed in glass bottom dishes in the presence of 2.5 μmol/L FM$^{®}$ 1-43 (Invitrogen$^{®}$, Grand Island, NY USA) with 1.5 mmol/L Ca^{2+}. Membrane damage was induced with a FluoView$^{®}$ FV1000 two-photon confocal laser-scanning microscope (Olympus, Center Valley, PA USA). A circular area (diameter, 5 μm) on the edge of the sarcolemma was irradiated at 20% power for 5 sec. Images were captured 5 sec prior to injury and every 5 sec after injury until 190 sec post irradiation. For every image, fluorescence intensity surrounding the site of damage was analyzed (ImageJ software, National Institute of Health, USA). The membrane repair assay was performed by a technician blinded to the mouse cohorts to reduce any potential for bias. Approximately 50 fibers per dose were analyzed.

Diaphragm tetanic contraction

As an additional outcome measure to the membrane repair assay, the diaphragms of systemically treated Bla/J mice were assessed at 20 weeks of age ($n = 6$ per dose). Mice were euthanized and the diaphragm was dissected with rib attachments and central tendon intact, and placed in K-H buffer at 37°C as previously described.[42,43] A 1–2 mm wide section (length from rib to tendon) of diaphragm was isolated and attached to a force transducer. The diaphragm strip was looped around a basket assembly attached to the transducer and the tendon was pierced by a pin. The muscle was stretched to optimal length for measurement of twitch contractions, and then allowed to rest for 10 min before initiation of the tetanic protocol. The tetanic protocol consists of a series of six tetanic contractions (20, 50, 80, 120, 150, 180 Hz) occurring at 2 min intervals, each

with duration of 250 msec. The force was recorded for each stimulus and normalized for muscle width and length.

Immunohistochemistry

Immunolabeling for dysferlin was performed on all transduced tissue to assess efficacy of gene transfer. For dysferlin detection, tissue sections (12 μm) were incubated with rabbit anti-human dysferlin monoclonal antibody (Romeo; Epitomics, Abcam Burlingame, CA USA) at 1:100 in blocking solution (10% goat serum, 0.1% Tween-20 in PBS) for 1 h at 25°C in a wet chamber. Sections were washed with PBS 3 × 20 min, reblocked, and then incubated for 45 min at 25°C with an Alexa 568 goat anti-rabbit antibody (Molecular Probes, Grand Island, NY USA) at a 1:250 dilution. Sections were washed in PBS for 3 × 20 min and mounted with Vectashield mounting medium (Vector Laboratories, Burlingame, CA USA). Images were captured with a Zeiss Axioskop2 Plus Microscope and Axiocam MRC5 camera (Zeiss, Thornwood, NY USA). Four random 20× images (each field with an average of 150 muscle fibers) were captured per muscle and the number of fibers with dysferlin labeling was counted and expressed as percent of total number of fibers.

Morphometrics

Centralized nuclei counts were performed on sections of muscle stained with hematoxylin and eosin (H&E) from treated animals. Four random 20× fields of 12 μm sections for each muscle were captured and the number of fibers with central nuclei counted and expressed as a percentage of the total number of fibers. Two-way analysis of variance (ANOVA) statistical analysis was performed to compare treatment effect on central nucleation ($P < 0.01$).

Western blot analysis

From each muscle, fresh-frozen serial tissue sections were taken for protein preparation. Muscle samples harvested from treated and control groups were compared with WT tissue for levels of vector-mediated dysferlin compared to endogenous dysferlin. Protein (15 μg) extracted from treated and control samples was separated by sodiumdodecyl sulfate polyacrylamide gel electrophoresis (SDS-PAGE) (3–8% Novex NuPAGE gradient gels, Invitrogen), blotted on PVDF (polyvinylidene fluoride) or nitrocellulose membrane and probed with NCL-Hamlet (Novocastra, Buffalo Grove, IL USA) primary antibody (for dysferlin) at a dilution of 1:1000, or γ-tubulin

antibody (Sigma-Aldrich, St. Louis, MO USA) at a dilution of 1:10,000 followed by horseradish-peroxidase (HRP) labeled goat anti-mouse IgG (1:5000; Millipore, Billerica, MA USA) or goat anti-rabbit IgG (1:5000; Millipore) and signal captured on Hyblot CL autoradiography film (Denville, Metuchen, NJ USA). Densitometry analysis was performed using ImageQuant TL (GE Healthcare Life Sciences, Pittsburgh, PA, USA).

Immunological assays

For NHPs, whole blood samples were collected biweekly and used for ELISA and enzyme-linked immunosorbent spot assay (ELISpot) to track immunological response to the viral capsid, AAVrh.74, and the dysferlin transgene product. ELISAs were performed in 96-well Nunc Maxisorb ELISA plates coated with 2×10^9 vg AAVrh.74 per well in carbonate buffer. Serum samples were diluted from 1:5 through 1:819,200 in blocking solution (5% nonfat dry milk, 1% normal goat serum [Invitrogen] in $PBS^{-/-}$) and added to wells for 1 h at room temperature. Sera from previously screened NHPs were used for controls. Goat anti-monkey IgG-HRP (Sigma) was used as the secondary antibody for 30 min at room temperature followed by exposure with Ultra TMB-ELISA solution (Thermo Scientific, Waltham, MA USA). Absorbance of wells at OD450 was measured and used to calculate titer of positive reaction.

Peripheral blood mononuclear cells (PBMCs) were separated from whole blood samples through density gradient centrifugation, as previously described.[44] Briefly, fresh blood samples are spun in a table-top centrifuge (Sorval Legend RT, Thermo Scientific) and the top plasma layer is removed and stored in $-80°C$ freezer. The remaining blood was mixed with $PBS^{-/-}$ (Invitrogen), underlayed with Ficoll-Paque (Fisher Scientific, Pittsburgh, PA USA) and spun for density gradient separation. The middle layer containing the PBMCs is then removed and subjected to various wash/spin cycles before a final resuspension in CellGro RPMI1640 media (Fisher) supplemented with 10% fetal calf serum (Fisher) and penicillin and streptomycin. PBMCs were then plated in IP filter plates (Millipore) at a density of 2×10^5 cells/well. IP plate wells were precoated with monoclonal antibody provided in monkey interferon-γ ELISpot kit (U-Cytech Biosciences, Utrecht, The Netherlands). Three peptide pools were used which were used for the AAVrh.74 capsid protein (Genemed Synthesis, San Antonio, TX) containing 34–36 peptides, each 18 amino acids long and overlapping by 11 residues. Ten peptide pools were used which encompass the dysferlin protein (Genemed Synthesis) containing 48 peptides, each 15 amino acids long and overlapping by 10 residues. Concanavalin A (Sigma) served as a positive control and 0.25% dimethylsulfoxide as a negative control. Peptides were added directly to the wells at a final concentration of 1 μg/mL. After the addition of PBMCs and peptides, the plate was incubated at 37°C in 5–7% CO_2 and 100% humidity for 36–48 h. Following incubation the plate was developed according to the manufacturer's protocol. Interferon-γ spot formation was counted using Immunospot software (Series 3B Analyzer; Cellular Technology, Ltd, Cleveland, OH).

Blood samples from the NHPs were analyzed monthly for chemistry panel and complete blood count (CBC) testing internally.

Results

AAVrh.74.Dysferlin.DV

We constructed a human dysferlin dual vector cassette driven by the muscle specific MHCK7 promoter (Fig. 1) with a chimeric intron included for augmented RNA processing. The dysferlin cDNA was divided into two discrete vectors containing either the 3′ or 5′ ends. The 5′ cassette contains the MHCK7 promoter, chimeric intron and the first 3370 bp of the dysferlin cDNA, while the 3′ cassette contains the end 3866 bp of the dysferlin cDNA and the native 3′UTR/polyadenylation sequence. Importantly, the two vectors contain a 1 kb overlap region in the dysferlin cDNA to facilitate recombination in vivo. The individual cassettes were packaged into an AAVrh.74 vector using standard transfection and purified. Both vectors were within the 4.7 kb packaging limit of AAV and full-length dysferlin protein was detected in skeletal muscle consistent with the proposed process of homologous recombi-
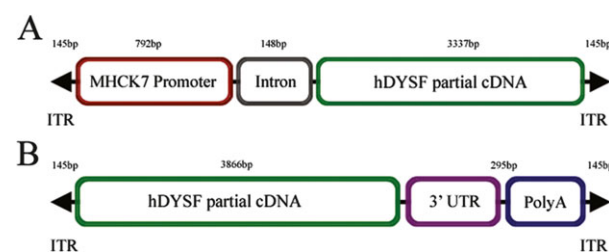

Figure 1. Schematic representation of dual vector dysferlin cDNA cassettes. (A) cDNA of pAAV.MHCK7.DYSF5′.PTG (PTG = promoter/transgene) containing the muscle specific MHCK7 promoter, chimeric intron to enhance gene expression, consensus Kozak sequence, and the first 3370 base pairs of the human dysferlin cDNA. The cDNA is flanked by AAV2 inverted terminal repeats (ITRs). (B) cDNA of pAAV.DYSF3′.POLYA containing the end 3866 base pairs of the dysferlin cDNA and the native 3′ UTR with a polyadenylation (PolyA) site. The overlap between the two cassettes consists of dysferlin cDNA bps 2407–3369. Both cassettes are packaged into AAVrh.74 for in vivo studies.

nation which occurs in transduced myocytes to generate the full-length dysferlin gene. Throughout the manuscript we refer to the constructs as AAVrh74.DYSF.DV, inclusive of both the 5′ and 3′ cassettes.

AAVrh.74.DYSF.DV gene transfer to limb muscles

IM delivery

As a continuation of our previous work,[16] we sought to study the long-term expression of dysferlin following gene transfer following fragment delivery with AAV5 or homologous overlap delivery with AAVrh.74.DYSF.DV. Intramuscular (IM) injections of 2×10^{11}vg AAV5.MHCK7.DYSF were performed in the left TA muscle of Dysf$^{-/-}$ mice. Mice were necropsied at 1, 3, 6, 9, and 12 months and TA sections were labeled for human dysferlin expression. Consistent, widespread expression was seen at all-time points tested (Table 1, Fig. S1). Western blot analysis showed a single, well-defined band at 237 kDa for the full-length protein at all-time points (Fig. S1).

As a direct comparison to AAV5.MHCK7.DYSF, we tested the ability of the AAVrh.74.DYSF.DV vectors to effectively transduce muscle fibers and express full-length dysferlin protein, we performed IM injections into the TA muscle of 4–6 week old 129-Dysf$^{-/-}$ at 2×10^{11}vg dose (1×10^{11}vg of each vector). Animals were sacrificed 1, 3, and 6 months postinjection and muscle sections were immunolabeled with anti-human dysferlin antibody and assessed for histopathological changes. As previously reported, Dysf$^{-/-}$ mice demonstrate mild pathology at young ages seen primarily in small numbers of centrally nucleated fibers and isolated necrotic fibers.[19,45] Following gene transfer with AAVrh.74.-DYSF.DV there was no evidence of toxicity in the treated muscles (Fig. 2A). Widespread dysferlin expression localized to the sarcolemma was detected through immu-nofluorescence and western blot of the treated TA tissue with no detectable dysferlin expression in contralateral control muscles (Fig. 2A). Quantification of muscle fibers expressing dysferlin at 1, 3, and 6 month demonstrated high levels of expression ($74 \pm 8.5\%$, $75.7 \pm 4.9\%$ and $90.5 \pm 1.5\%$, respectively; Table 1). This expression was an improvement as compared to our values using AAV5.DYSF (Table 1).[16] Western blot analysis showed a well-defined 237 kDa band for treated muscles which was absent for PBS control-treated animals (Fig. 2B). Densitometry analysis of the western blot normalized to γ-tubulin shows expression of dysferlin through dual vector at $86.8 \pm 1.7\%$ in comparison to wild type. This is an improvement over our previously published expression of dysferlin using AAV5 ($69.1 \pm 19\%$).[16] Additionally, TAs samples injected with AAVrh.74.DYSF5′.PTG, AAVrh.74.DYSF3′.PolyA, or AAVrh.74.DYSF.DV were screened for dysferlin protein production through western blot (Fig. S2). Importantly, no dysferlin protein (full-length or truncated) was detectable unless both the 5′ and 3′ viral preps were codelivered. This was also extensively studied through RNA analysis in our previous work with AAV5.-DYSF.[16]

Following necropsy at 3 or 6 months, the left and right TA along with organs (heart, lung, liver, kidney, spleen, and gonad) were harvested and analyzed for biodistribution of vgs. High levels of viral vector were detected in the left TA (treated) as expected; however, detectable levels were also found in all tissues tested (Fig. 2C and D). Importantly, western blotting of tissue lysates only found dysferlin protein expression in the injected left TA (not shown).

Regional vascular delivery

Given the robust expression of dysferlin upon IM delivery, we next tested the ability of the vectors to cross the vascular barrier and transduce muscle through an

Table 1. Dysferlin expression following IM delivery of AAVrh.74.MHCK7.DYSF.DV and AAV5.MHCK7.DYSF.

Test article (vector)	Animal strain	Dose	Endpoint (months)	Percent fibers expressing Dysf[1]
AAVrh.74.MHCK7.DYSF.DV	Dysf$^{-/-}$	2×10^{11}vg	1	$74.0 \pm 8.5\%$
			3	$75.7 \pm 4.9\%$
			6	$83.0 \pm 13\%$
AAV5.MHCK7.DYSF	Dysf$^{-/-}$	2×10^{11}vg	1	$67.3 \pm 16.4\%$
			3	$43.3 \pm 23.2\%$
			6	$46.4 \pm 18.3\%$
			9	$50.6 \pm 12.9\%$
			12	$58.0 \pm 13.7\%$

IM, intramuscular; Dysf, dysferlin.
[1]Four 20× fields were counted per muscle (~550–600 fibers per animal).

ILP procedure. We have previously shown that the rh.74 transduces muscle very efficiently when delivered through the vasculature.[25] This lays the foundation for future translation to clinical practice as it allows for treatment of multiple muscle groups. The lower left limb of 4–6 week old Dysf$^{-/-}$ mice was perfused with 2×10^{12}vg AAVrh.74.DYSF.DV (1×10^{12}vg of each vector) in 100 μL normal saline as previously described.[41] Animals were sacrificed 4 weeks postinjection to study dysferlin expression. Quantification of transduced muscles showed $68 \pm 15\%$ of fibers expressing dysferlin throughout the lower limb muscles (TA and gastrocnemius, Fig. 3).

Systemic vascular delivery

To test the feasibility and effectiveness of systemic delivery approach, we treated BlaJ (B.6A-Dysf^{prmd}/GeneJ, dysferlin deficient) mice with saline, 2×10^{12}vg, or 6×10^{12}vg total dose of AAVrh.74.DYSF.DV through tail vein injections. Animals were sacrificed at 3 months and analysis included diaphragm specific force measurements,

membrane repair analysis in the FDB muscle and full necropsies to quantify dysferlin expression and assess histopathology. Quantification of muscle fibers expressing dysferlin was performed in the TA, gastrocnemius, quadriceps, triceps, and diaphragm muscles. At 2×10^{12}vg, the muscles exhibited low level, variable expression, while the 6×10^{12}vg dose demonstrated widespread expression in all muscles (Table 2, Fig. 4). Whereas untreated BlaJ mice exhibit low levels of pathology at the time point studied, significant differences in fibers with centralized nuclei were calculated for the gastrocnemius muscle for both low and high dose treated animals. Diaphragm central nuclei counts for both doses were not significantly different from WT BL6 mice (Fig. 4).

Functional outcomes of dysferlin deficiency in skeletal muscle

Development of a clinically relevant therapeutic requires preclinical efficiency with functional outcome measures. We have previously demonstrated the use of a membrane repair assay for the FDB and specific force
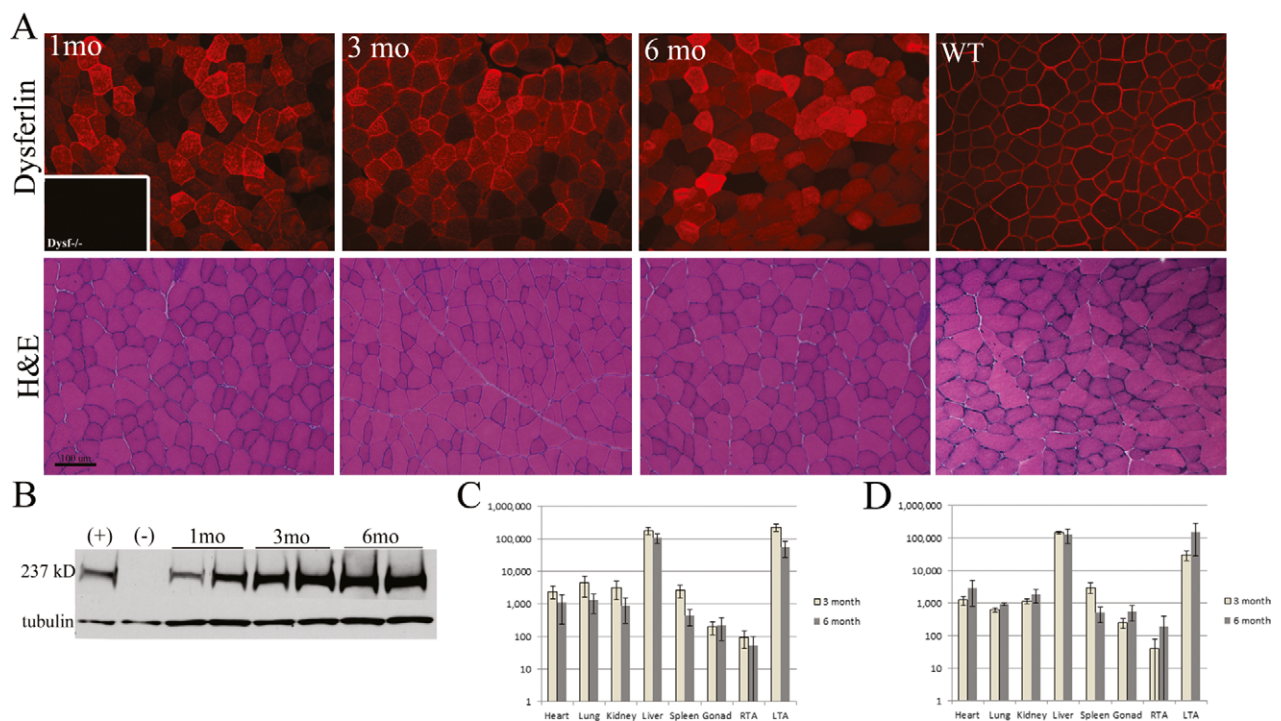

Figure 2. Dysferlin expression following intramuscular delivery of AAVrh.74.MHCK7.DYSF.DV. (A) Full-length dysferlin expression demonstrated by dysferlin immunolabeling seen following delivery of dual vectors to left tibialis anterior (LTA). Dysferlin expression persisted through 1, 3, and 6 months post-treatment with no aberrant response in pathology (H&E, lower panels). Scale bar, 100 μm. Wild-type dysferlin staining and histology is also included for comparison. Inset: contralateral saline treated tissue showing no dysferlin staining. $N = 4$ per timepoint (B) Western blot shown for 1, 3, 6 month samples demonstrating expression of full-length dysferlin in injected LTAs (2 per group). γ-tubulin used as loading control. (C and D) Biodistribution plot of vector genomes per μg genomic DNA at 3 and 6 months postinjection for (C) AAVrh.74.DYSF5′.PTG and (D) AAVrh.74.DYSF3′.PolyA. Note: the LTA was treated; logarithmic axis. Error bars represent standard error mean.
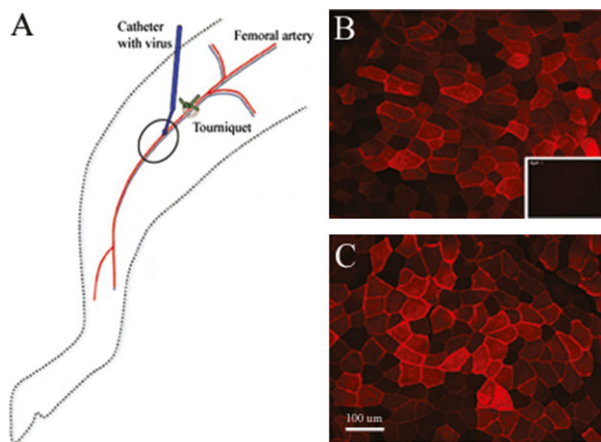
Figure 3. Isolated Limb Perfusion of Dysf$^{-/-}$ mice with AAVrh.74.-MHCK7.DYSF.DV. Dysferlin deficient mice (4–6 weeks of age) were perfused with AAVrh.74.MHCK7.DYSF.DV (1e12vg each vector) in 100 μL of normal saline ($n = 4$). (A) Schematic illustrating isolation of the lower femoral artery and procedure used to perfuse animals. Four weeks postgene transfer, animals were sacrificed and assessed for dysferlin expression. $68 \pm 15\%$ of muscle fibers were transduced throughout the lower limb muscles as compared to contralateral control (B, inset). Shown are (B) tibialis anterior (TA) and (C) gastrocnemius (GAS) muscles. Scale bar 100 μm.

Table 2. Quantification of dysferlin expression following systemic delivery of AAVrh.74.MHCK7.DYSF.DV.

Dose	2×10^{12}vg	6×10^{12}vg
	Percent fibers expressing Dysf[1]	
	Mean $\pm$ SD	
Muscle group	Low dose	High dose
Tibialis anterior	$3.2 \pm 3.6\%$	$14.2 \pm 6.3\%$
Gastrocnemius	$3.6 \pm 2.5\%$	$27.0 \pm 13.7\%$
Quadriceps	$3.2 \pm 2.1\%$	$18.5 \pm 12.4\%$
Triceps	$2.1 \pm 0.9\%$	$21.4 \pm 8.2\%$
Diaphragm	$6.3 \pm 3.7\%$	$25.0 \pm 6.2\%$

[1]Four 20× fields were counted per muscle (~550–600 fibers per animal).

measurements in the diaphragm as physiological outcome measures.[16]

Membrane repair

We next evaluated the ability of AAVrh.74.DYSF.DV to improve muscle fiber membrane repair ability in dysferlin deficient muscle. We performed a membrane wounding/resealing assay using a multiphoton laser scanning microscope on fibers isolated from the FDB. The experimental design allowed for blinding of the samples during the membrane repair assay to reduce any potential for bias. We tested FDBs from Dysf$^{-/-}$ mice treated by IM injection and from BlaJ mice treated by systemic delivery (described above). Dysf$^{-/-}$ mice at 8 weeks of age were injected IM with escalating doses of AAVrh.74.DYSF.DV (6×10^9, 2×10^{10}, and 6×10^{10}vg total dose) in the FDB. A control Dysf$^{-/-}$ cohort received saline and 129-WT mice served as strain specific normal controls. Animals were sacrificed 12 weeks after injections and FDBs were isolated and processed with collagenase to isolate individual fibers. Sarcolemmal damage was induced in isolated fibers using a multiphoton laser (20% power for 5 sec) in the presence of FM1-43 dye. A small area of fluorescence was detected for all fibers immediately after laser injury at the site of damage. In WT fibers, the fiber undergoes a normal repair process and the membrane is resealed halting the influx of dye. In dysferlin deficient

fibers, this repair process is altered, hindering the ability of the membrane to reseal, and thereby allowing a continuous influx of dye. Expression of dysferlin from AAVrh.74.DYSF.DV-transduced fibers resulted in a dose-dependent improvement in resealing capacity (Fig. 5). For the three treatment groups, only the high dose (6×10^{10}vg) restored repair to near WT levels (ANOVA). Parallel expression studies show high dose fiber transduction of $87 \pm 5.6\%$ (not shown).

The above work was repeated for FDBs extracted from systemically treated BlaJ mice (total doses of 2×10^{12} and 6×10^{12}vg). Again, individual muscle fibers were isolated and wounded using a multiphoton laser in the presence of FM1-43 dye. A dose-dependent response in resealing capability was observed, with the high dose (6×10^{12}vg) treated fibers showing repair not significantly different than WT. The low dose treatment (2×10^{12}vg) did not differ from untreated BlaJ (Fig. 6A).

Diaphragm physiology

Diaphragm strips from 3 month old BlaJ mice treated with saline, 2 or 6×10^{12}vg total dose of AAVrh.74.-DYSF.DV systemically were dissected with rib attachments and central tendon intact. A 1–2 mm wide section (from rib to tendon) of diaphragm was isolated and attached to a force transducer. Following stretching the muscle to optimal length for twitch contractions, the strip was subjected to a protocol of six tetanic contractions at 2 min intervals, each with duration of 250 msec to measure specific force. All measurements were normalized to cross-sectional area. Treated diaphragms exhibited significant improvement in force (ANOVA $P < 0.01$), which was not different from WT force at both doses (Fig. 6B).

Taken together, the diaphragm physiology and membrane repair data show that the large, potentially therapeutic dysferlin cDNA can be delivered to muscle and
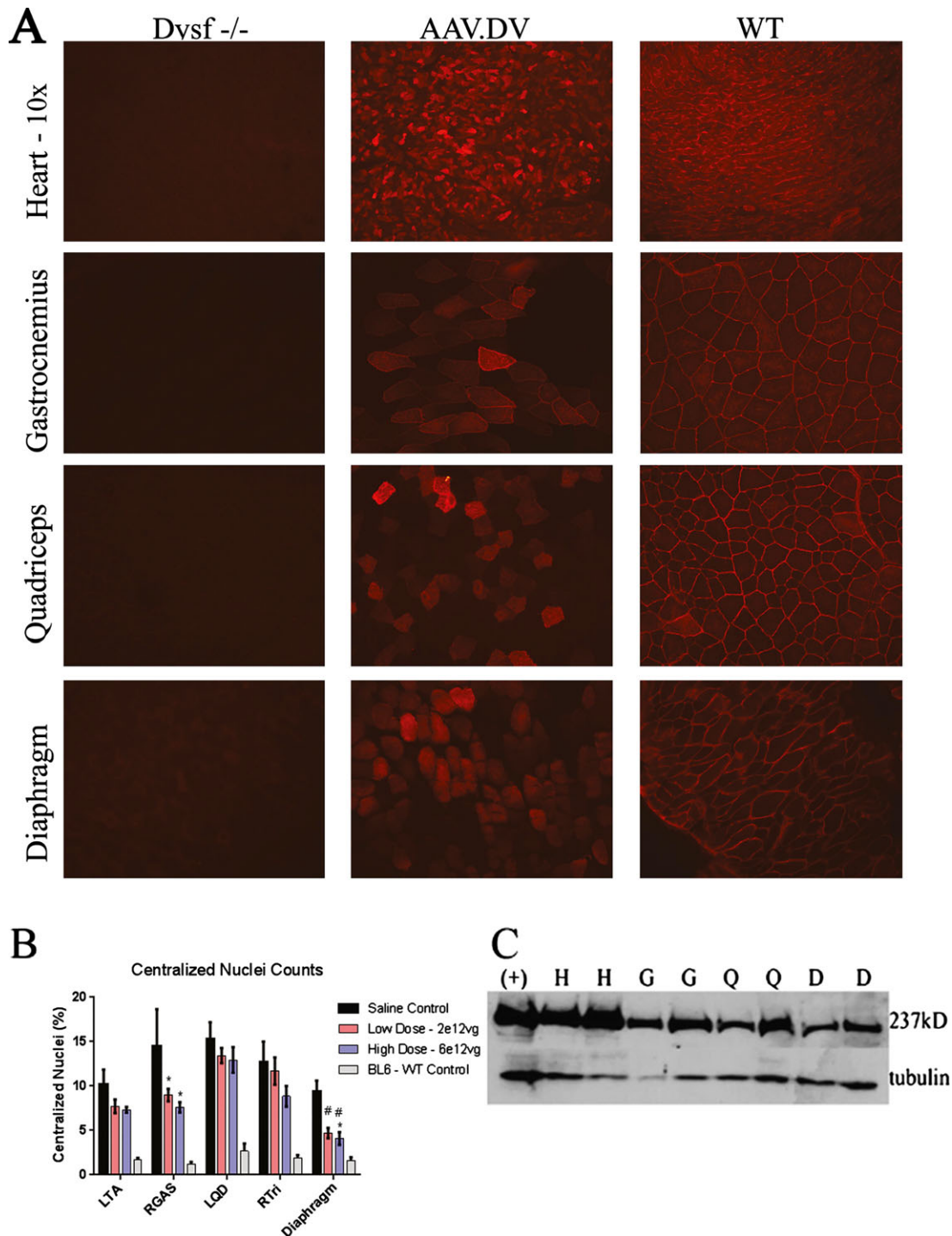
Figure 4. Dysferlin expression following systemic delivery of AAVrh.74.MHCK7.DYSF.DV. (A) Dysferlin immunolabeling of tissues after systemic delivery of 6×10^{12}vg AAVrh.74.MHCK7.DYSF.DV ($n = 6$ per dose). Muscles shown are heart, gastrocnemius, diaphragm, and quadriceps for Dysf$^{-/-}$, treated (AAV.DV) and wild-type (WT) tissues. (B) Quantification of centralized nuclei in the tibialis anterior (LTA), gastrocnemius (RGAS), quadriceps (LQD), triceps (RTri), and diaphragm. *$P < 0.05$ significant difference between sample and wild-type, #no significant difference between sample and wild-type. (C) Western blot of tissue lysates (H, heart; G, gastrocnemius; Q, quadriceps; D, diaphragm) demonstrating full length dysferlin band at 237 kD, γ-tubulin included as a loading control.
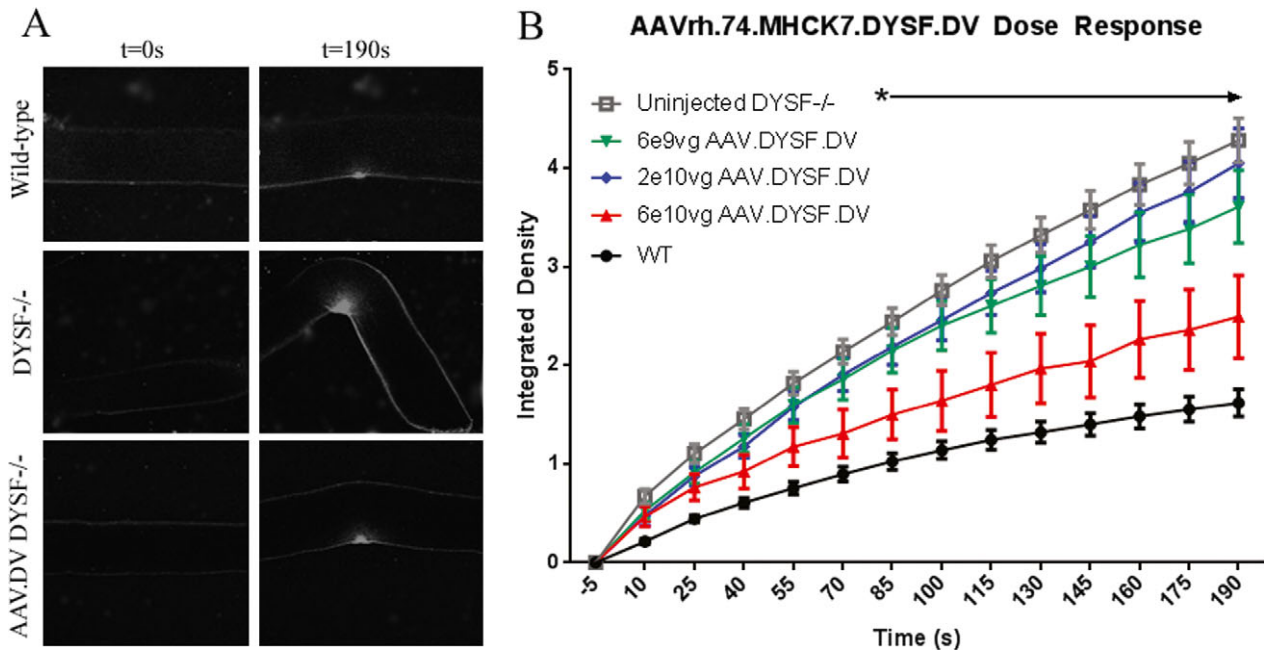
Figure 5. Dose-dependent membrane resealing activity following AAVrh.74.DYSF.DV delivery. Three doses of AAV vectors were injected into the FDB of 129-Dysf$^{-/-}$ mice at 8 weeks of age and analyzed 12 weeks post gene transfer at 20 weeks of age ($n = 6$ per group). A control Dysf$^{-/-}$ group received saline and a group of 129-WT mice served as strain specific normal controls. (A) Representative images preinjury (left column) and 190 sec postinjury (right column) of wild type, Dysf$^{-/-}$ and treated fibers. (B) Quantification of dye infiltration over time course of imaging. AAVrh.74.DYSF.DV treatment revealed dose dependent membrane resealing. Only the high dose (6e10vg) was not significantly different than WT (ANOVA). *Significant difference between high dose and uninjected Dysf$^{-/-}$. Error bars represent standard error mean.
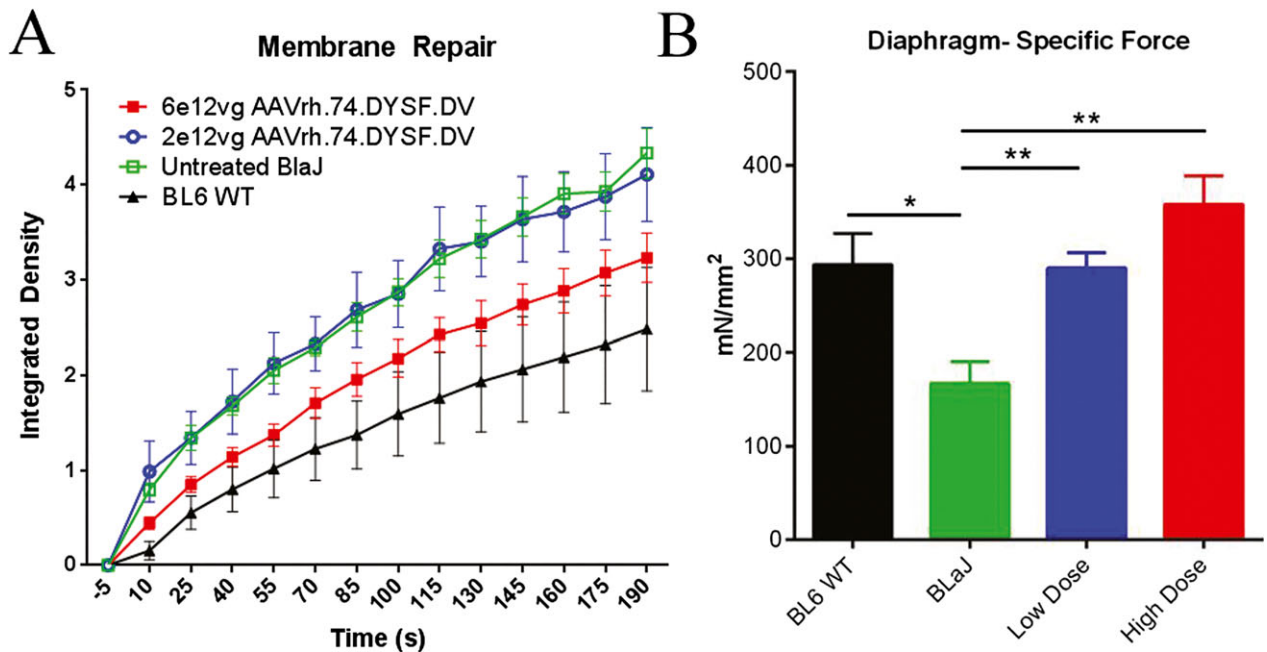

Figure 6. Systemic delivery of AAVrh.74.MHCK7.DYSF.DV restores functional deficits in BlaJ mice. (A) Membrane repair assay quantification. There was no significant improvement at low dose, however, high dose treatment restored repair to near wild-type levels (no significant difference). Error bars represent standard error mean. (B) Specific force generated by diaphragm muscle strips. Treated diaphragms demonstrated significant improvement in force (**$P < 0.01$, ANOVA) as compared to uninjected/untreated controls. Treated diaphragms were not statistically different from wild-type force at either dose.

efficiently express full-length, functional dysferlin using a dual-vector AAVrh.74 strategy.

AAV.DYSF gene transfer in NHPs

Translationally, it is important to apply the preclinical findings from work in mice to a clinical paradigm. As such, NHP offer a model with anatomic parallels to humans for safety and dosing considerations. We studied the effect of 5×10^{12}vg total dose delivered by IM injection to the left TA of both AAV5.DYSF ($n = 3$) and AAVrh.74.DYSF.DV ($n = 2$). Saline injected right

TA in the same animal served as a normal control. This dose was proportional (based on animal weight) to that given to mice. Baseline chemistries and immunological studies were performed, including ELISpot analysis to measure T cells against AAV5 and AAVrh.74 capsid and dysferlin as well as anti-AAV antibody titers (ELISA). These studies were repeated every 2 weeks for the entire study. Animals were euthanized 3 or 6 months following treatment for a full necropsy. Tissues were collected for gene expression studies including histopathology and biodistribution studies on vital organs. In both animal cohorts, the gene delivery
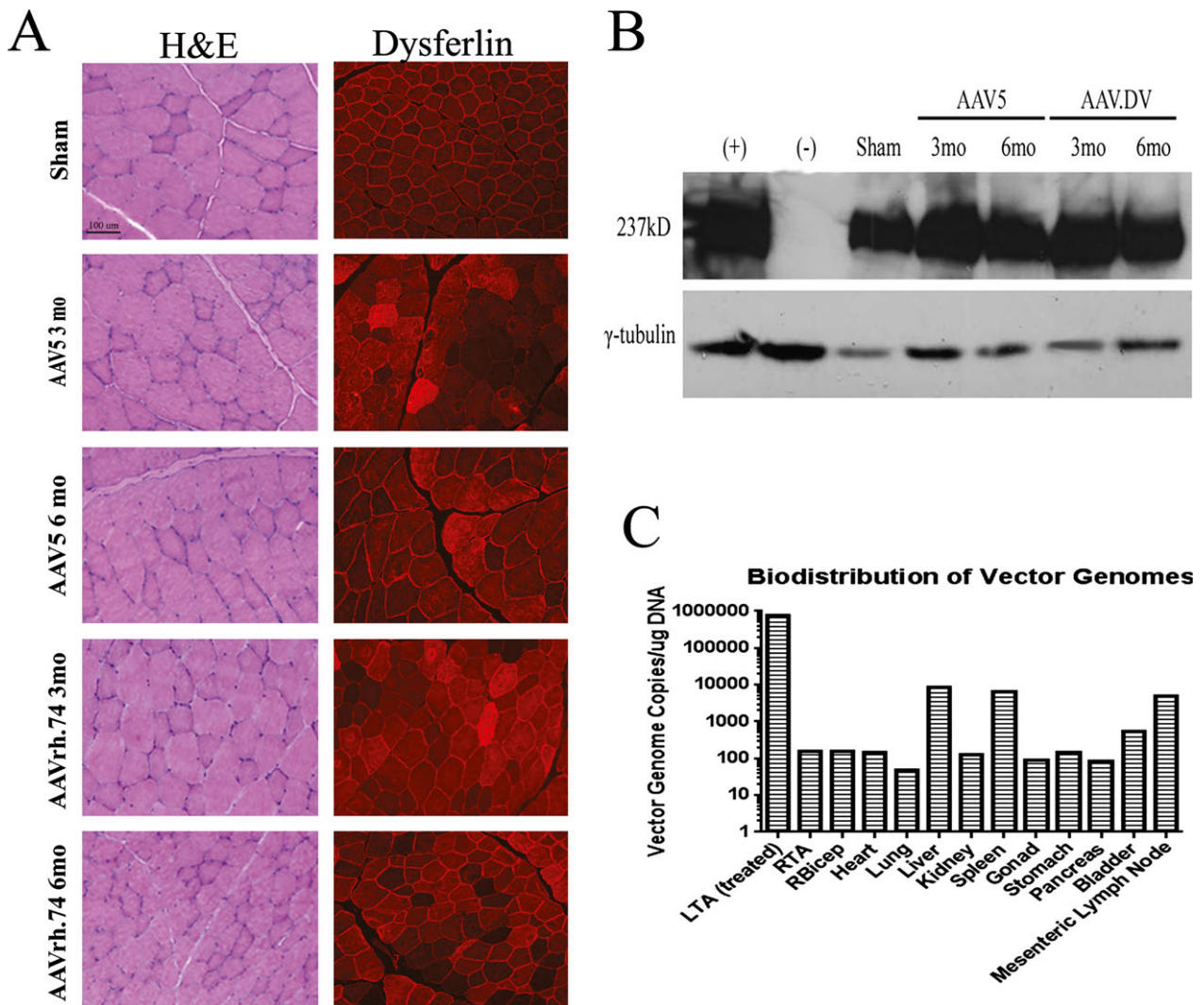

Figure 7. Dysferlin expression in nonhuman primates. (A) Histology (H&E) and dysferlin immunofluorescence (IF) images of NHP tissue at 3 and 6 months postinjection of either AAV5.DYSF or AAVrh.74.DYSF.DV. H&E stained sections show lack of immune infiltration and necrosis of fibers. IF sections show overexpression of dysferlin in injected tissues as compared to native (sham). (B) Western blot image of tissues from 3 and 6 months postinjection for both AAV5.DYSF and AAVrh.74.DYSF.DV. Importantly, injected tissues demonstrate an overexpression of dysferlin as compared to sham control. Positive (+) control is wild-type mouse tissue and the negative (−) control is 129-Dysf$^{-/-}$ uninjected tissue. (C) Biodistribution of vector genomes following IM injection with AAVrh.74.DYSF.DV into the left TA, note logarithmic scale.

resulted in robust expression of dysferlin in the injected muscle as compared to uninjected control (Fig. 7). Importantly, no toxicity was seen at the tissue level in the NHPs with a lack of inflammation or muscle fiber necrosis. For AAV5.DYSF injected TAs, the muscles demonstrated 104.9% (3 months) and 122.6% (6 months) overexpression of dysferlin while AAVrh.74.DV injected TAs had 122.0% (3 months) and 115.2% (6 months) overexpression as compared to the uninjected control. Immunological assays did not show any aberrant responses to the capsid or transgene by ELISpot (Fig. S3) or ELISA (Table S1). In addition full CBC and chemistry panels showed no abnormal values in any of the macaques.

Discussion

AAV-mediated gene therapy presents a desirable treatment strategy for multiple diseases; however, it is hindered by the restrictive 4.7 kb packaging limit of the AAV virion. Of particular interest are diseases with no current cure or effective therapy, such as dysferlinopathies. The work here provides proof that codelivery of two vectors allows for in vivo recombination events and production of full-length, functional dysferlin. Although there is discussion in the field as to the exact mechanism of dual vector treatments (i.e. repair vs. homologous recombination), our work with AAV5.DYSF,[16] and that of others,[29,37,38] points to homologous recombination of partially packaged genomes as the mechanism responsible for the generation of full-length transcripts. Work by Lostal et al. with designed splicing dual vectors showed low levels (1–4%) of dysferlin expression following systemic delivery of 4×10^{12}vg.[46] Here, we present similar levels of dysferlin expression (2–6%) following systemic delivery of 2×10^{12}vg indicating comparable efficiency between the two methods. Importantly, a threefold increase in dose dramatically improved expression levels (15–27%) and corresponding functional improvement. Additionally, comparison of AAV5.DYSF and AAVrh.74.-DYSF.DV expression in mice revealed an increase in dysferlin expression through the dual vector delivery. Regardless of mechanism, dual vectors utilizing either strategy are becoming a viable option for expression cassettes outside the traditional packaging limit of AAV.

Importantly, the work by Lostal et al. demonstrated the potential for DYSF gene replacement through a dual vector strategy.[46] Although they were only able to demonstrate low levels of dysferlin expression, this still resulted in an improvement in muscle pathology as well as an improvement in membrane repair. In their work, the low levels of dysferlin expression were not sufficient to restore functional measures to WT levels which led them to postulate that levels of 30% dysferlin expression would be necessary for clinically meaningful outcomes.[46] Following this work, we tested both low (2×10^{12}vg) and high (6×10^{12}vg) systemic doses of AAVrh.74.DYSF.DV leading to 2–6% and 15–27% dysferlin expression respectively. Functional outcome measures in membrane repair and diaphragm specific force were restored to WT levels for the high dose, suggesting that lower levels of expression (~25%) may be sufficient to see a clinical benefit. This is corroborated by considering carriers of DYSF mutations which have no clinical symptoms of dysferlinopathy but with <50% dysferlin protein expression.[47]

After demonstration of robust, wide-spread expression of dysferlin in mouse models, we moved the dual vector treatment strategy into rhesus macaques to study the efficacy and safety of such a therapy. Rhesus macaques and other NHPs have been used extensively as an approximation to a human response due to anatomic similarities.[25,48–53] As such, we studied not only the expression of dysferlin delivered by gene therapy, but also the systemic immunological response in the primates. Monitoring an immune response was critical as previous work demonstrated toxicity and progressive myopathy in cases of transgene overexpression.[39] In addition, previous work has shown that pre-existing immunity to the vector capsid results in diminished to absent expression of the transgene.[48] Thus, primates were prescreened prior to treatment for circulating binding antibodies to AAVrh.74, with only primates negative for AAV antibodies used for the study. We found that AAVrh.74.DYSF.DV treatment in macaque skeletal muscle can stimulate the overexpression of dysferlin with no apparent toxicity or systemic immune rejection, laying a foundation for preclinical safety. Potential immune responses were carefully monitored through both serum ELISAs and PBMCs ELISpot assays. Peptide pools used to stimulate the PBMCs were designed to be 15 amino acids long, overlapping by 10 amino acids so as to capture all possible antigenic epitopes. The lack of immune response shown in all of the primates is therefore encouraging. Our dose level led to thorough transduction of the treated muscle, which will guide our future toxicology studies as we prepare for clinical trial. A formal pre-IND discussion with the FDA (L. R. Rodino-Klapac and J. R. Mendell, pers. comm.) defined a potential path for a dysferlin dual vector clinical gene therapy trial providing no problems are encountered in planned toxicology/biodistribution studies done with the same rigor as other approved AAV vectors.[54–56]

In conclusion, our dual vector work is a promising therapeutic strategy for the treatment of dysferlinopathy patients. Comparison of the dual vector strategy with AAV5.DYSF demonstrated similar levels of expression and functional benefit with no increases in toxicity or

aberrant protein production. Furthermore, the success of multiple routes of delivery provides the option to vary treatment according to clinical presentation. The IM targeted therapy allows for the treatment of individual muscle groups affected in MM1 and distal anterior compartment myopathy, while the vascular and systemic delivery methods can be useful for gene delivery treatment of muscle compartments relevant to LGMD2B or MM1.

Acknowledgments

Author Contributions

P. C. S., D. A. G., E. R. P., W. E. G., R. W. J., Z. S., K. R. C., J. R. M., and L. R. R.-K. designed the study, performed experiments, and analyzed data. K. N. H., K. M. S., C. L. M., and J. L. performed experiments and analyzed data. P. C. S. and L. R. K. wrote the manuscript with contributions from all authors. J. R. M. and L. R. R.-K. obtained grant support.

Conflict of Interest

None declared.

References

1. Bashir R, Britton S, Strachan T, et al. A gene related to *Caenorhabditis elegans* spermatogenesis factor fer-1 is mutated in limb-girdle muscular dystrophy type 2B. Nat Genet 1998;20:37–42.

2. Liu J, Aoki M, Illa I, et al. Dysferlin, a novel skeletal muscle gene, is mutated in Miyoshi myopathy and limb girdle muscular dystrophy. Nat Genet 1998;20:31–36.

3. Illa I, Serrano-Munuera C, Gallardo E, et al. Distal anterior compartment myopathy: a dysferlin mutation causing a new muscular dystrophy phenotype. Ann Neurol 2001;49:130–134.

4. Rosales XQ, Gastier-Foster JM, Lewis S, et al. Novel diagnostic features of dysferlinopathies. Muscle Nerve 2010;42:14–21.

5. Seror P, Krahn M, Laforet P, et al. Complete fatty degeneration of lumbar erector spinae muscles caused by a primary dysferlinopathy. Muscle Nerve 2008;37:410–414.

6. Nagashima F, Chuma T, Mano Y, et al. Dysferlinopathy associated with rigid spine syndrome. Neuropathology 2004;24:341–346.

7. Urtizberea JA, Bassez G, Leturcq F, et al. Dysferlinopathies. Neurol India 2008;56:289–297.

8. Kobayashi K, Izawa T, Kuwamura M, Yamate J. Dysferlin and animal models for dysferlinopathy. J Toxicol Pathol 2012;25:135–147.

9. Klinge L, Dean A, Kress W, et al. Late onset in dysferlinopathy widens the clinical spectrum. Neuromuscul Disord 2008;18:288–290.

10. Nguyen K, Bassez G, Krahn M, et al. Phenotypic study in 40 patients with dysferlin gene mutations: high frequency of atypical phenotypes. Arch Neurol 2007;64:1176–1182.

11. Walter M, Reilich P, Thiele S, et al. Treatment of dysferlinopathy with deflazacort: a double-blind, placebo-controlled clinical trial. Orphanet J Rare Dis 2013;8:26.

12. Angelini C, Peterle E, Gaiani A, et al. Dysferlinopathy course and sportive activity: clues for possible treatment. Acta Myol 2011;30:127–132.

13. Lerario A, Cogiamanian F, Marchesi C, et al. Effects of rituximab in two patients with dysferlin-deficient muscular dystrophy. BMC Musculoskelet Disord 2010;11:1–7.

14. Aoki M, Liu J, Richard I, et al. Genomic organization of the dysferlin gene and novel mutations in Miyoshi myopathy. Neurology 2001;57:271–278.

15. Liu J, Wu C, Bossie K, et al. Generation of a 3-Mb PAC contig spanning the Miyoshi myopathy/limb-girdle muscular dystrophy (MM/LGMD2B) locus on chromosome 2p13. Genomics 1998;49:23–29.

16. Grose WE, Clark KR, Griffin D, et al. Homologous recombination mediates functional recovery of dysferlin deficiency following AAV5 gene transfer. PLoS One 2012;7: e39233.

17. Lek A, Lek M, North K, Cooper S. Phylogenetic analysis of ferlin genes reveals ancient eukaryotic origins. BMC Evol Biol 2010;10:231.

18. Abdullah N, Padmanarayana M, Marty N, Johnson C. Quantitation of the calcium and membrane binding properties of the C2 domains of dysferlin. Biophys J 2014;106:382–389.

19. Bansal D, Miyake K, Vogel SS, et al. Defective membrane repair in dysferlin-deficient muscular dystrophy. Nature 2003;423:168–172.

20. Lennon NJ, Kho A, Bacskai BJ, et al. Dysferlin interacts with annexins A1 and A2 and mediates sarcolemmal wound-healing. J Biol Chem 2003;278:50466–50473.

21. Lek A, Evesson F, Sutton B, et al. Ferlins: regulators of vesicle fusion for auditory neurotransmission, receptor trafficking and membrane repair. Traffic 2012;13:185–194.

22. Kerr J, Ward C, Bloch R. Dysferlin at transverse tubules regulates Ca^{2+} homeostasis in skeletal muscle. Front Physiol 2014;5:89.

23. Oulhen N, Onorato T, Ramos I, Wessel G. Dysferlin is essential for endocytosis in the sea star oocyte. Dev Biol 2014;388:94–102.

24. Fuson K, Rice A, Mahling R, et al. Alternate splicing of dysferlin C2A confers Ca²⁺-dependent and Ca²⁺-independent binding for membrane repair. Structure 2014;22:104–115.

25. Chicoine LG, Rodino-Klapac LR, Shao G, et al. Vascular delivery of rAAVrh74.MCK.GALGT2 to the gastrocnemius muscle of the rhesus macaque stimulates the expression of dystrophin and laminin alpha2 surrogates. Mol Ther 2014;22:713–724.

26. Gao G, Vandenberghe LH, Wilson JM. New recombinant serotypes of AAV vectors. Curr Gene Ther 2005;5:285–297.

27. Heller KN, Montgomery CL, Janssen PM, et al. AAV-mediated overexpression of human alpha7 integrin leads to histological and functional improvement in dystrophic mice. Mol Ther 2013;21:520–525.

28. Sahenk Z, Galloway G, Clark KR, et al. AAV1.NT-3 gene therapy for charcot-marie-tooth neuropathy. Mol Ther 2014;22:511–521.

29. Lai Y, Yue Y, Duan D. Evidence for the failure of adeno-associated virus serotype 5 to package a viral genome > or = 8.2 kb. Mol Ther 2010;18:75–79.

30. Allocca M, Doria M, Petrillo M, et al. Serotype-dependent packaging of large genes in adeno-associated viral vectors results in effective gene delivery in mice. J Clin Invest 2008;118:1955–1964.

31. Harper SQ, Hauser MA, DelloRusso C, et al. Modular flexibility of dystrophin: implications for gene therapy of Duchenne muscular dystrophy. Nat Med 2002;8:253–261.

32. Wells DJ, Wells KE, Asante EA, et al. Expression of human full-length and minidystrophin in transgenic mdx mice: implications for gene therapy of Duchenne muscular dystrophy. Hum Mol Genet 1995;4:1245–1250.

33. Duan D, Yue Y, Yan Z, Engelhardt JF. A new dual-vector approach to enhance recombinant adeno-associated virus-mediated gene expression through intermolecular cis activation. Nat Med 2000;6:595–598.

34. Ghosh A, Yue Y, Long C, et al. Efficient whole-body transduction with trans-splicing adeno-associated viral vectors. Mol Ther 2007;15:750–755.

35. Colella P, Trapani I, Cesi G, et al. Efficient gene delivery to the cone-enriched pig retina by dual AAV vectors. Gene Ther 2014;21:450–456.

36. Koo T, Popplewell L, Athanasopoulos T, Dickson G. Triple trans-splicing adeno-associated virus vectors capable of transferring the coding sequence for full-length dystrophin protein into dystrophic mice. Hum Gene Ther 2014;25:98–108.

37. Dong B, Nakai H, Xiao W. Characterization of genome integrity for oversized recombinant AAV vector. Mol Ther 2010;18:87–92.

38. Wu Z, Yang H, Colosi P. Effect of genome size on AAV vector packaging. Mol Ther 2010;18:80–86.

39. Glover L, Newton K, Krishnan G, et al. Dysferlin overexpression in skeletal muscle produces a progressive myopathy. Ann Neurol 2010;67:384–393.

40. Schnepp BC, Jensen RL, Chen CL, et al. Characterization of adeno-associated virus genomes isolated from human tissues. J Virol 2005;79:14793–14803.

41. Rodino-Klapac LR, Janssen PM, Montgomery CL, et al. A translational approach for limb vascular delivery of the micro-dystrophin gene without high volume or high pressure for treatment of Duchenne muscular dystrophy. J Transl Med 2007;5:45.

42. Rafael-Fortney JA, Chimanji NS, Schill KE, et al. Early treatment with lisinopril and spironolactone preserves cardiac and skeletal muscle in Duchenne muscular dystrophy mice. Circulation 2011;124:582–588.

43. Beastrom N, Lu H, Macke A, et al. mdx(cv) mice manifest more severe muscle dysfunction and diaphragm force deficits than do mdx mice. Am J Pathol 2011;179:2464–2474.

44. Labikova J, Vcelakova J, Ulmannova T, et al. The cytokine production of peripheral blood mononuclear cells reflects the autoantibody profile of patients suffering from type 1 diabetes. Cytokine 2014;69:189–195.

45. Ho M, Post CM, Donahue LR, et al. Disruption of muscle membrane and phenotype divergence in two novel mouse models of dysferlin deficiency. Hum Mol Genet 2004;13:1999–2010.

46. Lostal W, Bartoli M, Bourg N, et al. Efficient recovery of dysferlin deficiency by dual adeno-associated vector-mediated gene transfer. Hum Mol Genet 2010;19:1897–1907.

47. Fanin M, Nascimbeni A, Angelini C. Muscle protein analysis in the detection of heterozygotes for recessive limb girdle muscular dystrophy type 2B and 2E. Neuromuscul Disord 2006;16:792–799.

48. Chicoine LG, Montgomery CL, Bremer WG, et al. Plasmapheresis eliminates the negative impact of AAV antibodies on microdystrophin gene expression following vascular delivery. Mol Ther 2014;22:338–347.

49. Kota J, Handy CR, Haidet AM, et al. Follistatin gene delivery enhances muscle growth and strength in nonhuman primates. Sci Transl Med 2009;1:6ra15.

50. Rodino-Klapac LR, Montgomery CL, Bremer WG, et al. Persistent expression of FLAG-tagged micro dystrophin in nonhuman primates following intramuscular and vascular delivery. Mol Ther 2010;18:109–117.

51. Rodino-Klapac LR, Montgomery CL, Mendell JR, Chicoine LG. AAV-mediated gene therapy to the isolated limb in rhesus macaques. Methods Mol Biol 2011;709:287–298.

52. Pahl L, Schubert S, Skawran B, et al. 1,25-Dihydroxyvitamin D decreases HTRA1 promoter activity in the rhesus monkey–a plausible explanation for the

influence of vitamin D on age-related macular degeneration? Exp Eye Res 2013;116:234–239.

53. Sheppard N, Jones R, Burwitz B, et al. Vaccination against endogenous retrotransposable element consensus sequences does not protect rhesus macaques from SIVsmE660 infection and replication. PLoS One 2014;9:e92012.

54. Mendell JR, Rodino-Klapac LR, Rosales-Quintero X, et al. Limb-girdle muscular dystrophy type 2D gene therapy restores alpha-sarcoglycan and associated proteins. Ann Neurol 2009;66:290–297.

55. Mendell JR, Campbell K, Rodino-Klapac L, et al. Dystrophin immunity in Duchenne's muscular dystrophy. N Engl J Med 2010;363:1429–1437.

56. Mendell JR, Rodino-Klapac LR, Rosales XQ, et al. Sustained alpha-sarcoglycan gene expression after gene transfer in limb-girdle muscular dystrophy, type 2D. Ann Neurol 2010;68:629–638.

Supporting Information

Additional Supporting Information may be found in the online version of this article:

Figure S1. Long-term dysferlin expression following AAV5 delivery. Four week old 129Dysf$^{-/-}$ mice were injected with 2×10^{11} vg. AAV5.DYSF into the tibialis anterior muscle and necropsied at 1, 3, 6, 9, and 12 months. Western blot demonstrates dysferlin expression at 3, 6, 9, and 12 month timepoints (2 per group shown).

Figure S2. AAVrh.74.DYSF.DV single injections. Western blot of TA samples following injection with AAVrh.74.-DYSF5′.PTG, AAVrh.74.DYSF3′.PolyA, or AAVrh.74.DYSF.DV. Only co-injection of both vectors (AAVrh.74.-DYSF.DV) results in the production of full-length dysferlin. Injections of either AAVrh.74.DYSF5′.PTG or AAVrh.74.-DYSF3′.PolyA result in no protein production (full-length or otherwise). Both C-terminal (Romeo) and N-terminal (NCL-Hamlet) antibodies were used to identify no partial fragments of dysferlin were present (NCL-Hamlet blot shown).

Figure S3. Immunological response of primates to AAV5.DYSF and AAVrh.74.DYSF.DV intramuscular injection. Peripheral blood mononuclear cells were isolated and exposed to peptides comprising the AAV5 and AAVrh.74 capsid (blue bars) as well as human dysferlin (green). Cells reacting to the peptides release interferon-γ, quantified as spots through an ELISpot assay. Spots per million cells were counted with 50 spots/1×10^6 cells as the positive reaction threshold. Transient responses to both capsid and transgene are seen, however, there is a lack of sustained immune response. Note: positive control levels typically range 1000–3000 spots/1×10^6 cells. SPC, spot forming colonies

Table S1. AAV capsid binding antibody ELISA. Serum was isolated from primates biweekly and analyzed for binding antibody titer. Titer reported corresponds to last dilution at which ratio of response ≥two should be two words. two fold above background.

270